ESTCP

GUIDANCE DOCUMENT

# Integration of Sorting and Composition Control Process with Subsequent Stereo Lithography Apparatus Enabled Investment Casting

Diran Apelian
Jianyu Liang
***Worcester Polytechnic Institute***

Brandon McWilliams
***Army Research Laboratory***

**November 2022**

**ESTCP Project WP18-1176**

# REPORT DOCUMENTATION PAGE

*Form Approved*
*OMB No. 0704-0188*



| **1. REPORT DATE** *(DD-MM-YYYY)* | **2. REPORT TYPE** | **3. DATES COVERED** *(From - To)* |
|---|---|---|
| 30/11/2022 | SERDP Guidance Document | 6/4/2018 - 6/4/2023 |

**4. TITLE AND SUBTITLE**

Integration of Sorting and Composition Control Process with Subsequent Stereo Lithography Apparatus Enabled Investment Casting

**5a. CONTRACT NUMBER**
16-C-0020

**5b. GRANT NUMBER**

**5c. PROGRAM ELEMENT NUMBER**

**6. AUTHOR(S)**
Diran Apelian
Jianyu Liang
Worcester Polytechnic Institute

Brandon McWilliams
Army Research Laboratory

**5d. PROJECT NUMBER**
WP18-1176

**5e. TASK NUMBER**

**5f. WORK UNIT NUMBER**

**7. PERFORMING ORGANIZATION NAME(S) AND ADDRESS(ES)**
Worcester Polytechnic Institute
Washburn Labs 329
100 Institute Road
Worcester, WA 01609

**8. PERFORMING ORGANIZATION REPORT NUMBER**
WP18-1176

**9. SPONSORING/MONITORING AGENCY NAME(S) AND ADDRESS(ES)**
Strategic Environmental Research and Development Program (SERDP)
4800 Mark Center Drive, Suite 16F16
Alexandria, VA 22350-3605

**10. SPONSOR/MONITOR'S ACRONYM(S)**
SERDP

**11. SPONSOR/MONITOR'S REPORT NUMBER(S)**
WP18-1176

**12. DISTRIBUTION/AVAILABILITY STATEMENT**
DISTRIBUTION STATEMENT A. Approved for public release: distribution unlimited.

**13. SUPPLEMENTARY NOTES**

**14. ABSTRACT**
An experimental methodology utilizing limited reductant kinetic experiments is proposed that can be analyzed using the solution (Eq.25 or 27) of the kinetic Eqs.14 and 17. The results are second order rate constants and the quantity of reductant available at the experimental conditions of the reaction. These parameters can then be used to investigate which of the experimental conditions are affecting magnitude of the second order rate constant, the reductant concentrations and the resulting first order rate constant.

**15. SUBJECT TERMS**
Second Order Rate Constants, Reactive Reductant Concentrations, Limited Reductant Kinetic Experiments

| **16. SECURITY CLASSIFICATION OF:** | | | **17. LIMITATION OF ABSTRACT** | **18. NUMBER OF PAGES** | **19a. NAME OF RESPONSIBLE PERSON** |
|---|---|---|---|---|---|
| **a. REPORT** | **b. ABSTRACT** | **c. THIS PAGE** | | | Diran Apelian |
| UNCLASS | UNCLASS | UNCLASS | UNCLASS | 30 | **19b. TELEPHONE NUMBER** *(Include area code)* 508-831-5992 |

# GUIDANCE DOCUMENT

Project: WP18-1176

## TABLE OF CONTENTS

# LIST OF FIGURES

**Page**

# LIST OF TABLES

**Page**

# ACRONYMS AND ABBREVIATIONS

| | |
|---|---|
| 3D | three-dimensional |
| AISI | American Iron and Steel Institute |
| ARL | Army Research Laboratory |
| C | carbon |
| CE | Carbon Equivalent |
| CT | computed tomography |
| DEVCOM | U.S. Army Combat Capabilities Development Command |
| DI | Ideal Critical Diameter |
| GVSC | Ground Vehicle System Center |
| h | hour |
| HRC | Rockwell hardness |
| HV | Vickers hardness test |
| ksi | kilo-pound per square inch |
| kW | kilowatt |
| mm | millimeter(s) |
| Mn | manganese |
| nm | nanometer(s) |
| OES | Optical Emission Spectroscopy |
| SFSA | Steel Founders' Society of America |
| Si | silicone |
| SLA | stereo lithography apparatus |
| TGA | thermal gravimetric analysis |
| UTS | ultimate tensile strength |
| WPI | Worcester Polytechnic Institute |
| YS | yield strength |

## 1. Characterization and sorting of the ferrous waste materials representative of those found on a forward-operating base

2567.08 lbs. of waste metal from the U.S. Army Combat Capabilities Development Command-Army Research Laboratory (DEVCOM-ARL) have been received. For each waste part, the chemical composition was characterized by Optical Emission Spectroscopy (OES). Information, such as weight, dimensions, contamination, and pictures, was also recorded in a waste material database as shown in Figure 1. The obtained composition information is stored in a database that can be accessed in a cloud folder. In addition, a separate database is maintained by the research team that reflects the change in the available waste material due to melting experiments.

## 2. Blending model and protocol for composition control

| Numerical Order | Picture of Scrap | Categorization | Dimensions (Approximate, Overall Size) | Contamination | Weight (lbs.) | info/note | Fe | C | Si | Mn | P | S | Cr | Mo | Ni | Al | Co | Cu |
|---|---|---|---|---|---|---|---|---|---|---|---|---|---|---|---|---|---|---|
| 2-1 |  | Hydraulic | 27" x 10" | Coating, Partial, Plastic Comp, Hydraulic Fuel | 14.14 | Hydraulic Fuel Inside | 99.5 | 0.0551 | 0.012 | 0.188 | 0.0217 | 0.0117 | 0.0398 | <0.003 | <0.005 | 0.0357 | 0.002 | 0.0201 |
| 2-2 |  | Exhaust Pipe | 22" x 6" | Partial Rust | 6.49 | | 99.5 | 0.0616 | <0.005 | 0.273 | 0.024 | / | / | <0.005 | <0.005 | 0.0294 | 0.0061 | 0.03 |
| 2-3 |  | Tank | 20" x 10" x 6" | Partial Rust, Coating, Plastic Comp. | 6.17 | | 99.2 | 0.0887 | 0.0117 | 0.513 | 0.0154 | 0.0091 | 0.0378 | <0.003 | 0.0119 | 0.0373 | 0.0029 | 0.0357 |
| 2-4 |  | Conduit Box | 18.75" x13.5" x 4.75" | Coating, Partial Rust, Internal Components | 15.47 | | 99.6 | 0.0619 | <0.005 | 0.178 | 0.0272 | 0.0199 | 0.0122 | <0.003 | 0.0069 | 0.0186 | 0.0041 | 0.0112 |
| 2-5 |  | ) Gallon Drum L | 23.5" x 1" | Entirely Covered in Rust | 6.18 | | 99.5 | 0.0698 | 0.0095 | 0.224 | 0.0094 | 0.0122 | 0.0326 | 0.0032 | 0.0073 | 0.0414 | 0.0027 | 0.0441 |
| 2-6 |  | ollow Square Tu | 8 x 4 1/8 x 8 3/8 | Partial Rust | 6.03 | | 98.7 | 0.248 | 0.0064 | 0.818 | 0.0262 | 0.015 | 0.0136 | <0.003 | <0.005 | 0.042 | 0.0035 | 0.0181 |
| 2-7 |  | Brake Rotor | 10 7/8 x 3 1/4 | Entirely Covered in Rust | 9.34 | | 86.8 | 0.0292 | 0.462 | 0.206 | 0.0023 | <0.002 | 12 | 0.0464 | 0.0934 | 0.0109 | 0.0143 | 0.0988 |
| 2-8 |  | C Channel | 6" x 6.25" x 1 7/8" | Entirely Covered in Rust | 4.1 | | 98 | 0.141 | 0.191 | 0.679 | 0.0274 | 0.0591 | 0.144 | 0.0168 | 0.128 | < 0.002 | 0.0071 | 0.602 |

*Figure 1. Part of waste material database.*

A blending model, guiding the selection and mixing of the waste materials to create the targeted steel alloy was developed using the MATLAB programming language. A text document with instructions on using the blending model was created to effectively teach new users in using the

blending model. This blending model has been shared with the research team members at Worcester Polytechnic Institute (WPI) and DEVCOM-ARL.

Using the blending model, a spreadsheet similar to that shown in Figure 2 can be generated. In this spreadsheet, the targeting composition and mechanical properties are specified. The selected waste materials and their weight, their corresponding compositions, and the range of expected composition for the formulated new alloy from these selected waste materials are also specified. In addition to the composition range of each alloying element, Ideal Critical Diameter (DI) and Carbon Equivalent (CE) are included in the blending model for improved control of mechanical properties. DI is used for representing the hardenability of a steel, and CE is used to indicate the response of the alloy in avoiding cracks caused by welding. Both factors can be calculated from the chemical composition of a given sample. DI and CE were proven to be useful in estimating the mechanical properties of as-cast steel. The generated formulation from waste metals must meet both the composition range and the targeted DI and CE for high confidence in obtaining the desirable hardness.

| Steel 1 Carbon Steel 45 ksi YS | | | | | | | | | | | | | | | | | | |
|---|---|---|---|---|---|---|---|---|---|---|---|---|---|---|---|---|---|---|
| | | | | CE | DI | % C | % Si | % Mn | % P | % S | % Cr | % Mo | % Ni | %Al | %Co | %Cu | %V | %Sn |
| | Recovery | | | | | 0.9 | 0.95 | 0.95 | 1.0 | 1.0 | 0.97 | 0.99 | 0.99 | 1.0 | 1.0 | 1.0 | 1.0 | 1.0 |
| | Target Composition | | Aim | 0.40 | 0.80 | | | | | | | | | | | | | |
| | | | Min | | 0.60 | 0.15 | 0.40 | 0.50 | | | 0 | 0 | 0 | | | | | |
| | | | Max | 0.50 | 0.90 | 0.30 | 0.60 | 1.20 | 0.035 | 0.035 | 0.50 | 0.20 | 0.50 | | | | | |
| | Heat Composition | | | 0.43 | 0.89 | 0.147 | 0.506 | 0.768 | 0.021 | 0.013 | 0.190 | 0.054 | 0.343 | 0.015 | 0.005 | 0.180 | 0.009 | 0.011 |
| | Heat Size (lb.) | | 70 | | | | | | | | | | | | | | | |
| | | | | | | | | | | | | | | | | | | |
| Waste Parts | Name | Remain | Added (lb.) | Fraction | Dimensions | % C | % Si | % Mn | % P | % S | % Cr | % Mo | % Ni | %Al | %Co | %Cu | %V | %Sn |
| #3-35 | Plate with Square Hole | 45.400 | 54.600 | 0.780 | 27.75" x 15.125" x 1.0" | 0.136 | 0.050 | 0.809 | 0.017 | 0.008 | 0.077 | 0.014 | 0.084 | 0.019 | 0.003 | 0.188 | | 0.009 |
| #4-15 | Big Thread Barrel 5 | 32.780 | 10.000 | 0.143 | 4.5" x 24" | 0.355 | 0.320 | 0.739 | 0.055 | 0.022 | 0.879 | 0.284 | 1.870 | | 0.017 | 0.090 | 0.052 | 0.020 |
| #3-32 | Big L Beam | 27.810 | 5.000 | 0.071 | 3.0" x 3.0" x 64.0" | 0.087 | 0.270 | 0.972 | 0.002 | 0.048 | 0.123 | 0.037 | 0.189 | | 0.009 | 0.284 | 0.022 | 0.015 |

*Figure 2. A screenshot of the waste material blending model.*

## 3. Demonstration: fabricating 8640, 4140 alloy steel, and 1025 carbon steel from waste materials

The team conducted successful melting experiments using the received waste materials, guided by the blending model, to create 8640, 4140, and 1025 alloys. Table 1 summarizes the target compositions and obtained compositions of these melts.

*Table 1. Target composition and obtained composition 8640, 4140 alloy steel, and 1025 carbon steel melts.*

| | | C | Mn | Si | Cr | Mo | Ni | S | P | DI | CE |
|---|---|---|---|---|---|---|---|---|---|---|---|
| Target: 8640 | Min. | 0.38 | 0.75 | 0.3 | 0.4 | 0.15 | 0.4 | 0 | 0 | 4.44 | 0.64 |
| | Max. | 0.43 | 1 | 0.6 | 0.6 | 0.25 | 0.7 | 0.04 | 0.035 | 8.38 | 0.81 |
| As-cast Composition | | 0.43 | 0.7 | 0.57 | 0.75 | 0.19 | 0.66 | 0.016 | 0.019 | 8.06 | 0.78 |
| Target: 4140 | Min. | 0.38 | 0.75 | 0.15 | 0.8 | 0.15 | / | 0 | 0 | 5.09 | 0.69 |
| | Max. | 0.43 | 1 | 0.3 | 1.1 | 0.25 | / | 0.04 | 0.035 | 8.15 | 0.87 |
| As-cast Composition | | 0.414 | 0.805 | 0.153 | 1.12 | 0.215 | 0.527 | 0.039 | 0.023 | 7.05 | 0.81 |
| Target: 1025 | Min. | 0.22 | 0.3 | / | / | / | / | 0 | 0 | 0.23 | 0.27 |
| | Max. | 0.28 | 0.6 | / | / | / | / | 0.05 | 0.04 | 0.45 | 0.38 |
| As-cast Composition | | 0.25 | 0.65 | 0.32 | 0.34 | 0.11 | 0.43 | 0.016 | 0.029 | 0.43 | 0.36 |

The three melts in compositions closely match the targeted compositions. This validated that the developed blending model serves as an effective guiding tool for rationally formulating waste materials for remelting in order to obtain new alloys with desirable mechanical properties.

Mechanical properties of as-cast steels were characterized by tensile tests following ASTM E8 standard (Tension testing of metallic materials). Figure 3 shows the sample E8 subsize tensile

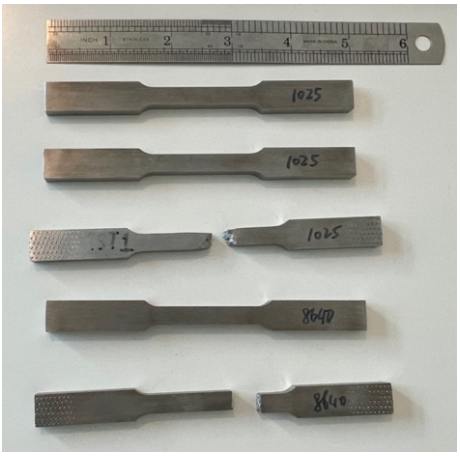


*Figure 3. E8 subsize tensile bar samples for tension testing.*

bars made from as-cast ingots. Table 2 shows the measured tensile properties of as-cast 1025 and 8640 samples. Table 2 also includes the ranges of reported tensile properties of as-cast 1025 and

8640 alloys that the team managed to find. Test results in Figure 4 and Table 2 show that the measured mechanical properties agree with the range of reported values.

*Table 2. Mechanical properties measured and reported range of value of as-cast 1025 and 8640 steel [1, 2].*

| | | Tensile Strength (ksi) | Yield Strength (ksi) |
|---|---|---|---|
| As-cast 1025 | Range of reported value | 73–83 | 33–45 |
| | Measured | 80.10 | 48.75 |
| As-cast 8640 | Range of reported value | 110–130 | 83–120 |
| | Measured | 114.71 | 81.78 |

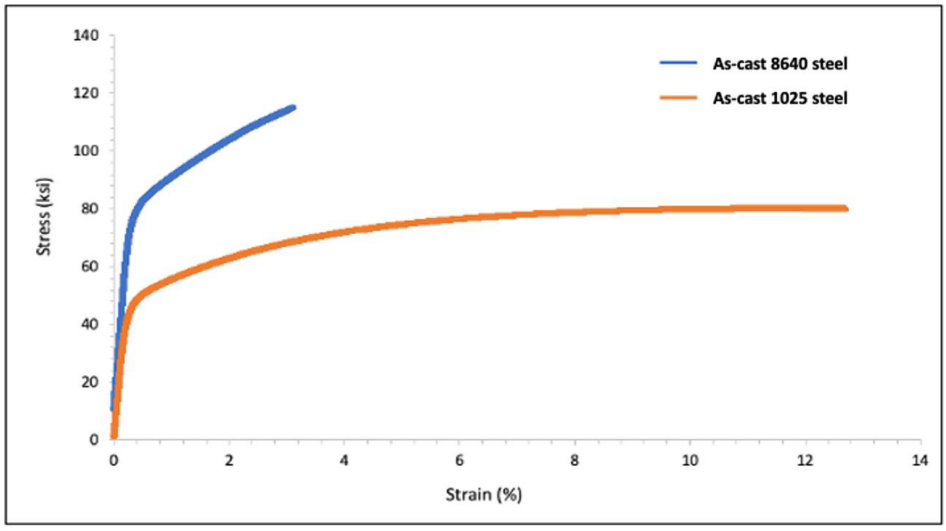


*Figure 4. Tensile testing results for as-cast 8640 alloy steel and 1025 carbon steel (engineering stress vs. engineering strain).*

It is worth pointing out that the microstructure and properties of as-cast steel material are profoundly affected by the solidification process. The outer layer of the cast is significantly supercooled while the inner region is cooled at a milder temperature gradient. As-cast steel products generally consist of serious dendrite segregation, uneven microstructures, and coarse grains. It must be heat-treated before it can be used in any application. The cast product is generally delivered after it has been heat-treated. The heat-treatment process can manipulate the mechanical property effectively. Literature research found that the as-cast tensile properties usually were not considered reliable indicators of the mechanical properties of the final products.

In steel-making literature, it is usually the post-heat treatment properties that are reported. In addition, sparsely reported tensile properties of as-cast steels varied across large ranges, as seen in Table 2.

It is well-known that making steel tensile samples is a time-consuming and challenging process. It is desirable to substitute the tensile test with the non-destructive hardness test for steel material characterization. A hardness test requires minimum sample preparation. In addition, a microhardness indenter is a desktop instrument that can be easily fitted into a mobile foundry with limited space. It is easy to use, easy to calibrate, and easy to maintain. Thus, in this project, instead of focusing on tensile measurements, the team collaborated with the Steel Founders' Society of America (SFSA) to study the correlation of yield strength, tensile strength, hardness, and chemical composition of steel materials. Using over 30,000 data entries collected by SFSA from steel foundries all over the United States over many years, this project has shown that hardness can be used to estimate yield strength (YS) and ultimate tensile strength (UTS) of steel. The standard errors of the established correlation were 10.7 ksi for YS and 6.05 ksi for UTS. The result of this data-driven study agrees with the previous reported linear correlation between steel tensile properties and hardness. This part of the work has been discussed in previous quarterly reports and will be included in the final report.

Thus, in this part of the study, the hardness of as-cast samples was characterized by microhardness indenter and used as the primary mechanical property indicator. The hardness values of as-cast product were measured in ten different locations for each sample to reduce the influence of nonuniform microstructures. Vickers hardness test (HV) results of all three steel alloys are summarized in Table 3, which also shows the ranges of sparsely reported hardness values of these alloys from the literature. The measured hardness of all three alloys appears to be in good agreement with the range of reported values. However, the variations in the reported values are very large. In addition, heat treatments will alter the mechanical properties of the steel alloys significantly. In the later section of this report, the heat treatments applied to the three demonstration components and the hardness of the heat-treated final products are discussed.

The success in multiple melts using the blending model that incorporates useful tools such as DI and CE in addition to individual alloy element composition confirms the feasibility of composition monitoring and adjustment of waste steel melts using the waste material database.

*Table 3. Hardness measured and reported range of as-cast 1025, 8640 and 4140 steel. [1-5].*

| | As-cast 1025 | As-cast 8640 | As-cast 4140 |
|---|---|---|---|
| Reported hardness range (HV) | 131–150 | 174–286 | 180–332 |
| Measured hardness (HV) | 139 | 292 | 303 |

## 4. Fabrication of investment casting patterns

### *4.1 Stereo lithography apparatus (SLA) printers*

There were two stereo lithography apparatus (SLA) printers used in this project: 3D System ProJet 6000 HD, which is typically used in industrial applications and mass production; and Formlabs Form 2, which is a low-cost, desktop printer. Figure 5 shows these two SLA printers side by side.

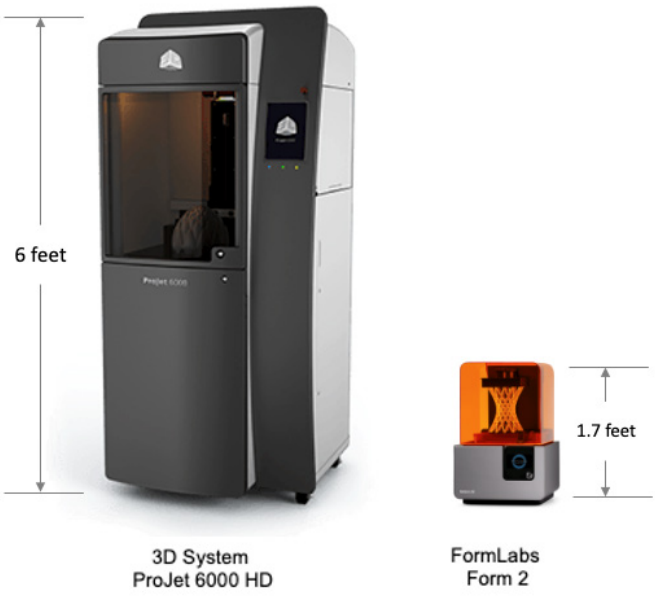


*Figure 5. Two SLA printers used in the project: 3D System ProJet 6000HD and Formlabs Form 2.*

The ProJet 6000 HD will take up more space in the compact foundry, but it is more reliable and suitable for batch manufacturing with a higher printing speed. It also provides a higher xy

accuracy at 25 micrometers. Formlabs Form 2 has a much smaller footprint and lighter weight. Additionally, Formlabs Form 2 is available at a lower price, which is less than one-fifth of the price of the 3D System ProJet 6000HD. Formlabs Form 2 is also easier to operate and costs less to maintain. However, its xy accuracy is limited at 140 micrometers. Technical specifications of the two printers are compared in Table 4 [1, 2].

*Table 4. Technical specifications comparison: 3D System ProJet 6000 HD and Formlabs Form 2 [1, 2].*

| Model (Brand) | ProJet 6000 HD (3D System ) | Form 2 (FormLabs) |
|---|---|---|
| Dimensions (mm) | 787*737*1829 | 350*350*520 |
| Weight (kg) | 181 | 13 |
| Min. Layer Thickness (mm) | 0.05 | 0.03 |
| XY Accuracy (mm) | 0.025 | 0.14 |
| Max. Biuld Size (mm) | 250*250*250 | 146*145*175 |
| Price ($) | 185,000 | 3,499 |

*4.2 Pre-printing design for investment casting patterns*

The patterns used in investment casting must be printed in a hollow structure. The hollow structure of the patterns can reduce the amount of material used, avoid cracks in the ceramic shell caused by polymer expansion during the burnout process, and maintain sufficient strength in the patterns. In the 3D System printing software, there is a built-in hollow function. Using this function, the parts can be meshed into honeycomb-supported, hollow structures. However, there is not such a function in the Formlabs printing software. Therefore, in order to print out hollow structures with Formlabs printers, other software such as AutoMeshmixer needs to be used to hollow the parts before printing. The optimization of the SLA process will be summarized in the next report, which specifically focuses on the next task in this project, optimizing the SLA enabled IC. Figure 6 shows the optimized Part #12446263 hollow pattern for printing with the Formlabs printer.

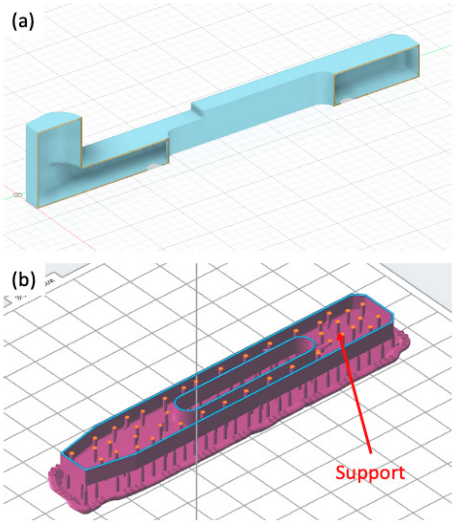


*Figure 6. (a) Part#12446263 hollow pattern cross-section view, (b) internal supports created by Preform.*

### *4.3 Printing of investment casting patterns*

The DEVCOM-ARL-WPI team has selected three workpieces to demonstrate the SLA enabled investment casting process. The engineering drawings of the three components were provided by the U.S. Army DEVCOM Ground Vehicle System Center (DEVCOM-GVSC). Part #12314649 patterns were printed with 3D system 6000HD. Part #12446263 and Part #154072 patterns were printed with Formlabs Form 2. The chamber size of the furnace for burnout at WPI is limited to 6in.*5in.*5in. The size of Part #154072 is higher than 6 inches, which exceeds the capacity of the furnace. Therefore, for Part #154072 the team scaled the component proportionally by 50% for demonstration purposes.

As shown in Figure 7 (a), Part #12314649 patterns were printed with a 3D System ProJet 6000HD, using VisiJet clear resin by the ARL team. The Part #12446263 and Part #154072

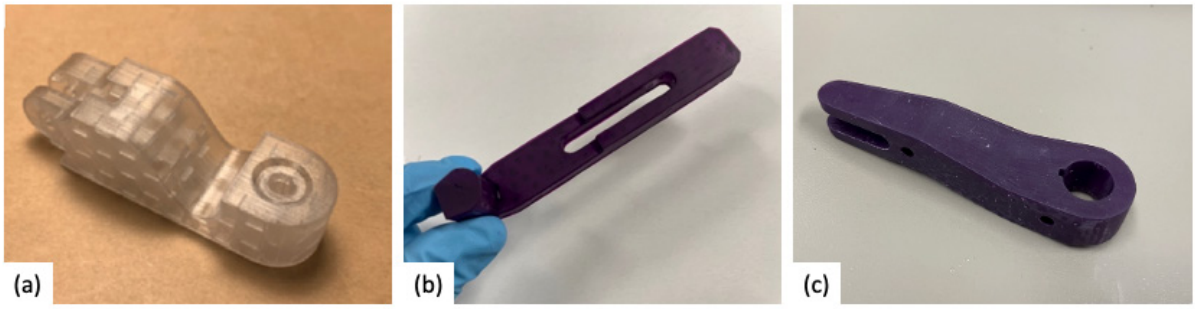


*Figure 7. (a) Part #12314649 hollow pattern printed with 3D System Project 600HD; (b) Part#12446263 hollow pattern printed with Formlabs Form 2; (c) Part #154072 hollow pattern printed with Formlabs Form 2.*

patterns were printed with Formlabs Form 2 using Castable Wax, by the WPI team as shown in Figure 7 (b, c). A machine stock of 0.06 inches was included in the design of the polymer patterns, and this portion of material can be easily machined after casting. The holes on the workpieces are castable. However, the tolerance requirements of these features still demand machining after casting. Thus, different cast patterns were made with and without holes. For the design without holes, the cast piece was machined to create the required holes.

Normally, investment cast steel parts will shrink by 1%~2.5% after solidification [3, 4], primarily due to the melting of the wax mold, the expansion of the ceramic shell, and the shrinkage of the metal after cooling. In this project, shrinkage factors from 2% to 3% have been experimented with SLA pattern designs. After trials, a shrinkage factor of 3% was used for the final SLA pattern design.

## 5. Investment casting tree assembly design and simulation

Generally, in manufacturing settings, casting "trees" are not produced in a single step. Instead, delicate master patterns are made separately and then assembled onto a universal stem, as shown in Figure 8. Since the stem in a casting tree is only used as sprue and runners, it does not require high accuracy and can be made of wax at lower cost.

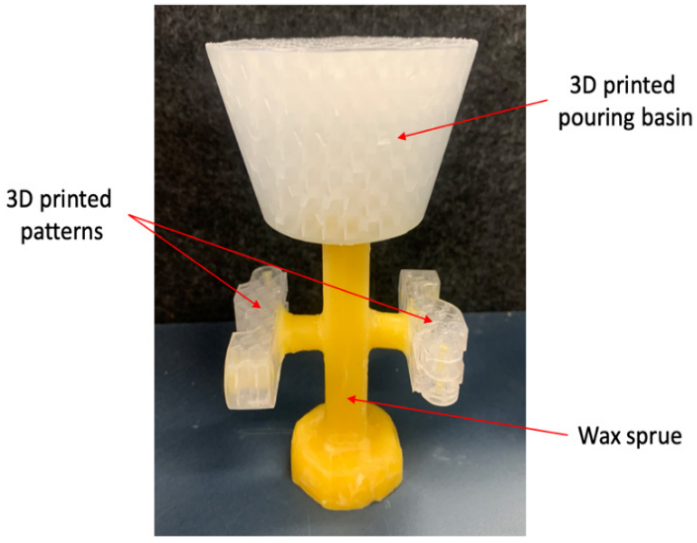


*Figure 8. Casting tree assembly of Part #12314649.*

The team designed the casting tree for three demonstration parts, based on the MagmaSoft simulation results. MagmaSoft is one of the most commonly used finite-element analysis

software programs in the metal-casting industry. It can simulate temperature and flow during pouring and solidification. In the simulation, the team focused on porosity and hot spots, which are two major defects in a cast part. Hot spots are sections of casting that cool down more slowly than the surrounding material. Any hot spot causes abnormal shrinkage in its vicinity, which can lead to porosity and cracking.

Multiple simulations were conducted. Based on the simulation results, optimized designs were created to avoid possible defects. For example, for Part #12314649, as shown in Figure 9 (a), runners had been added on the sides of the sprue to connect the parts. By doing so, metal flow would first fill the buffer zone at the bottom of the casting tree, and then fill the workpiece cavity at a gentle speed. As shown in Figure 9 (b, c), simulation confirmed that in the optimized design there was no porosity or hot spots in the workpieces. The defects were located in the pouring basin and sprue, which would not affect the quality of the final products. Figures 10 and 11 show the final cast tree design for the other two demo parts.

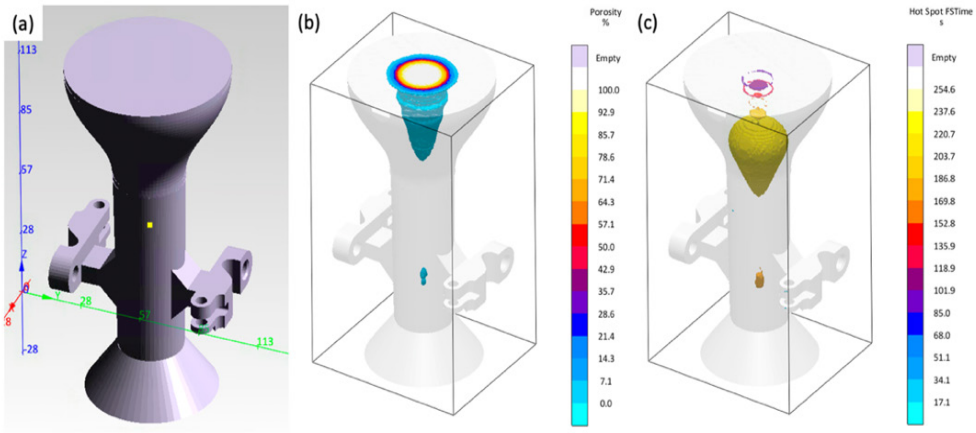


*Figure 9. (a) Casting tree design for Part #12314649; (b) Porosity simulation result; and (c) Hot spot simulation result.*

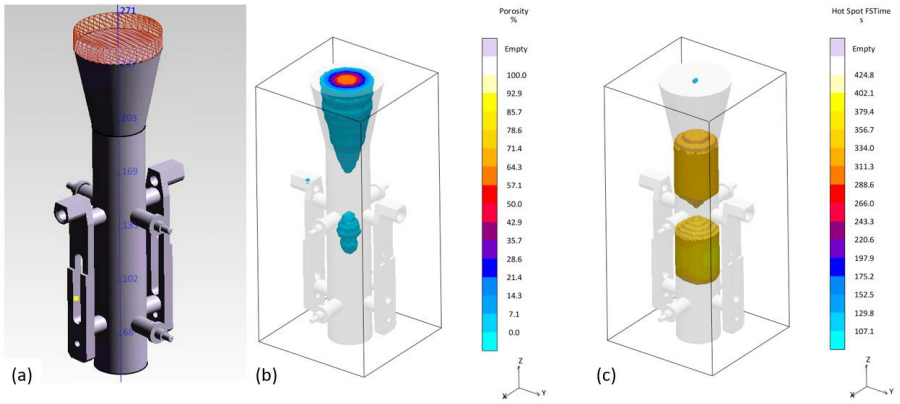


*Figure 10. (a) Casting pattern design for Part #12446263; (b) Porosity simulation result; and (c) hot-spot simulation result.*

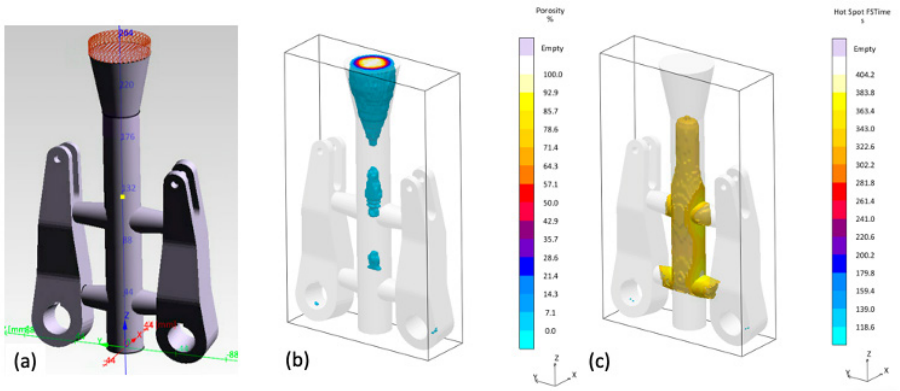


*Figure 11. (a) Casting pattern design for Part #12446263; (b) Porosity simulation result; and (c) hot-spot simulation result.*

Figures12 and 13 show the casting tree assembly of Part #12446263 and Part #154072.

*Figure 12. Casting tree assembly of Part #12446263.*

*Figure 13. Casting tree assembly of Part #154072.*

## 6. Ceramic shell making and burnout

The ceramic shell was made by a 6-layer dipping and stucco process to ensure sufficient strength during burnout and casting as documented in previous reports. All the refractory materials used to make the ceramic shell were purchased from Remet. Briefly, first, the zirconium silicate-based slurry was prepared. In this slurry system, Remet WET-IN provides good wetting of waxes, fast wetting-in of slurry refractories and does not degrade slurry life. LUDOX® HS-30 is a colloidal silica with an average particle size of 12 nm. It works as a binder and provides high strength to the ceramic shell after burnout. A wetting agent was also added to improve the adhesion between the slurry and stucco material.

Table 5 summarizes the shell-making process. A completed ceramic shell is shown in Figure 14. The shell thickness was measured as 4.1mm.

*Table 5. Stucco sequence for ceramic shell production.*

| Layer | Slurry | Stucco Material |
|---|---|---|
| 1 | Primary | Zircon Sand |
| 2 | Primary | Zircon Sand |
| 3 | Primary | Mulgrain 47 60S |
| 4 | Primary | Mulgrain 47 60S |
| 5 | Primary | Mulgrain 47 22S |
| 6 | Primary | Mulgrain 47 22S |

*Figure 14. Completed ceramic shell before burnout.*

After the ceramic shell was dried, the shell is placed in a burnout furnace. As shown in Figure 15, a 36-hour burnout schedule was developed and verified to be sufficient to fully remove the SLA-printed polymer patterns. The burnout schedule consisted of three distinct stages. First, the ceramic shell was heated to 90°C at 30°C/h and held for 3 hours. At this temperature, the ceramic shell became hardened, and the wax sprue and the SLA patterns started to degrade. The

slow ramping-up rate allowed the materials to heat up slowly, reducing the chance of cracking in the ceramic shell. Secondly, the ceramic shell was heated to 155°C at 30°C/h and held for 3 hours. At this temperature, the moisture in the shell was fully removed, and the SLA patterns continued to degrade. Lastly, the shell was heated to 675°C at 45°C/h and held for 3 hours. According to the thermal gravimetric analysis (TGA) results shown in Figure 16, both VisiJet Clear Resin and Formlabs Castable Wax completely decomposed at 650°C. After this stage, the ceramic shell was slowly cooled to room temperature at 60°C/h.

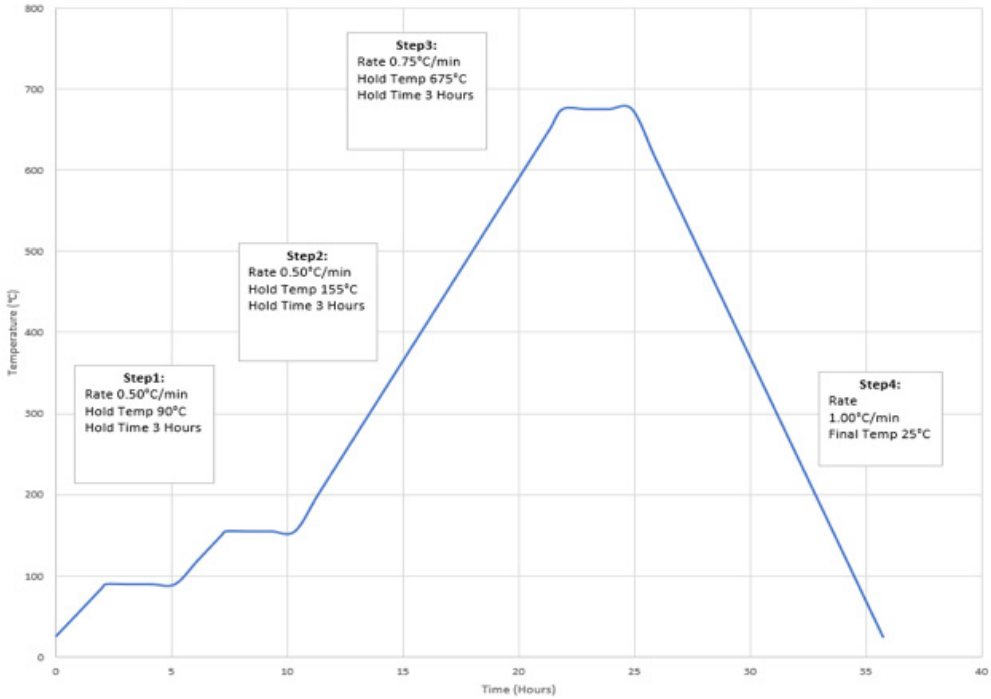


*Figure 15. Burnout schedule designed for ceramic shell production.*

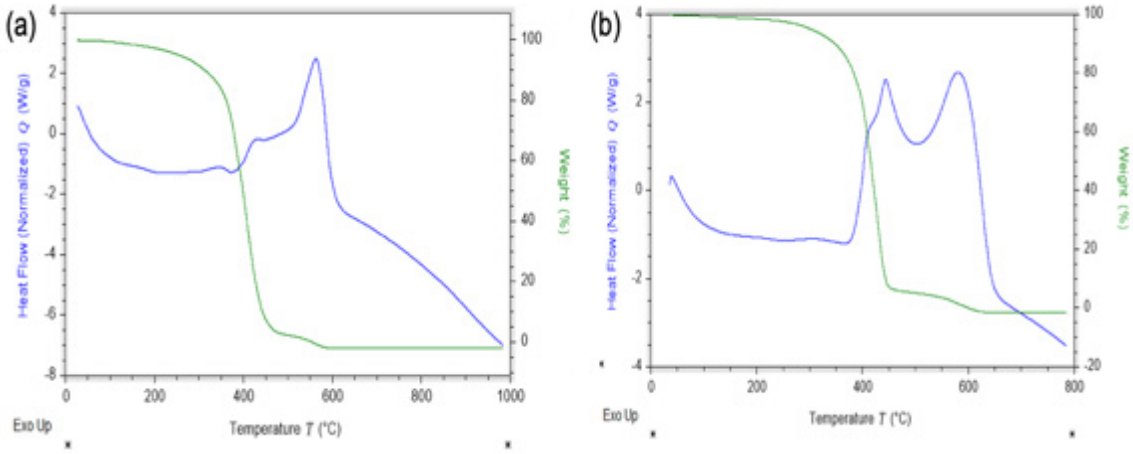


*Figure 16. TGA results of (a) VisiJet castable resin and (b)Formlabs castable wax.*

As shown in Figure 17, no cracking was observed in the ceramic shell after burnout. Computed tomography (CT) scan results in Figure 18 confirmed that the resin was completely decomposed, and a clean cavity was obtained. To ensure that no cracks or residual resin remained in the ceramic shell, the ceramic shell (after burnout) was cut in half to carefully evaluate the internal surface. As shown in Figure 19, there was no resin residue found on the surfaces, in corners, or along the edges of the shell. The overall geometry of the cavity was smooth and complete. This result confirms that the dipping, stucco, and burnout processes were effective for the required ceramic shell production. The internal geometry of the ceramic mold replicated all the design features well.

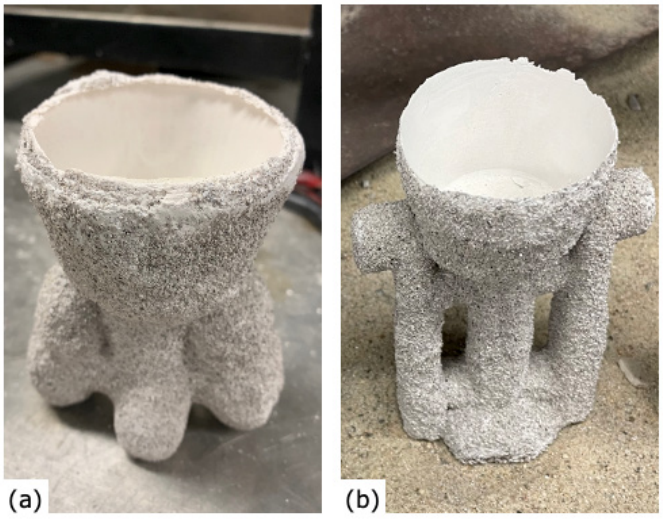


*Figure 17. Ceramic shells after burnout (a) Part#12314649 casting tree assembly; (b) Part#12446263 casting tree assembly.*

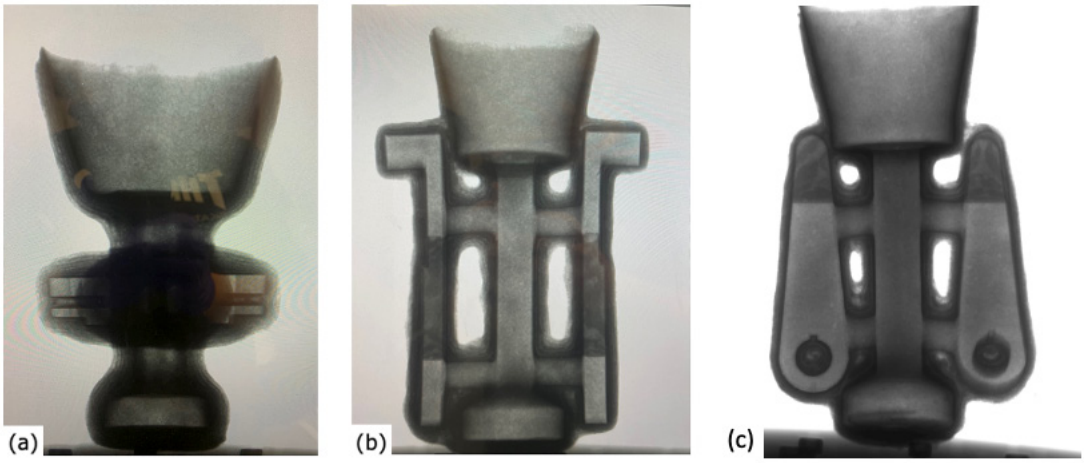


*Figure 18. CT scan results of ceramic shells after burnout: (a) Part#12314649 casting tree assembly; (b) Part#12446263 casting tree assembly; (c)Part#154072 casting tree assembly.*

*Figure 19. Ceramic shell (after burnout) is cut in half to carefully evaluate the internal surface.*

## 7. Casting process

As shown in Table 6, the melting process consists of four stages. After adding the steel waste material into the crucible, the furnace power was ramped up to 17kW. This stage was used to

*Table 6. Melting time using Inductotherm Mini-Melt furnace.*

| Time (Minutes) | Power (kW) | Action |
|---|---|---|
| 0 | 0 | Add waste material into crucible |
| 0-30 | 17 | Crucible preheat |
| 30-90 | 30 | Main melting stage |
| 90-110 | 25 | Conduct composition analysis, adjust composition |
| 110-140 | 30 | Temperature measuring, pouring |

preheat the crucible, to prevent damage from too-rapid heating. This preheating stage lasted at least 30 minutes, until the waste metal pieces were heated to around 700°C and became red in color. Then, the power was increased to 30kW for the melting stage. At this stage, materials were completely converted into molten metal. The melting time and crucible power were adjusted, based on the total amount of waste metal. A steel rod was used to stir the molten metal

occasionally, to ensure proper mixing, and a skimmer was used to remove slag formed during melting. Figure 20 shows some of the tools used during the melting process.

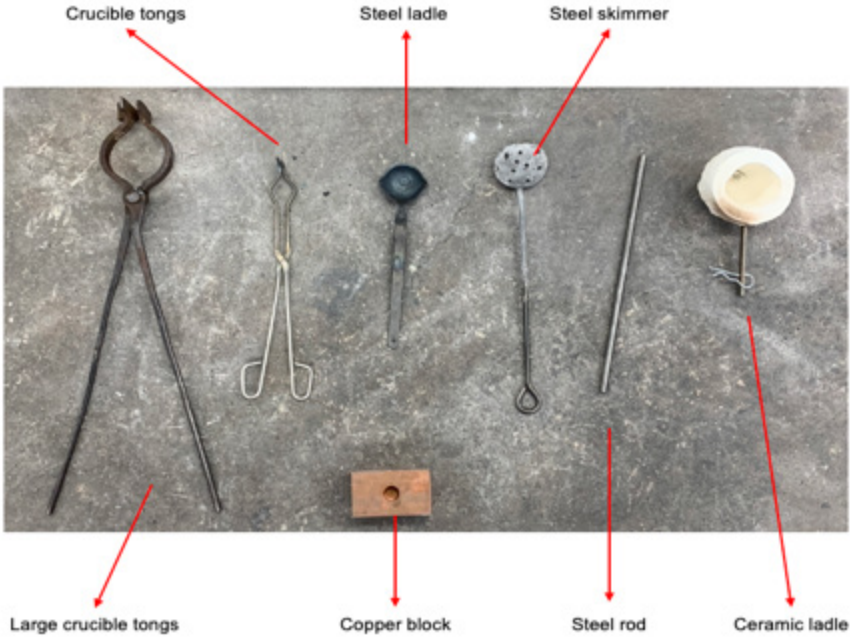


*Figure 20. Tools utilized in the melting and pouring process.*

After this stage, the furnace power was reduced to 25kW while conducting composition analysis, using portable OES. A small amount of metal was scooped and poured into a copper mold with a 1-inch depth and 1-inch diameter cavity. The large difference in the thermal expansion coefficient between steel and copper makes it easy to remove the steel sample from the cavity for OES tests. Based on the OES test result and the alloy composition requirement, small amounts of other materials were added into the crucible for chemical composition adjustment. Then, the furnace power was increased back to 30kW. The objective of this stage was to heat the molten metal to the target pouring temperature of 1650°C. An immersion pyrometer was used for temperature monitoring during the melting process. Once the temperature of the molten metal reached 1650°C uniformly, the metal melt was ready to be poured into ceramic shells.

Before pouring, the ceramic shell was preheated in a furnace at 1100°C and held for at least 2 hours. The preheating was conducted in parallel with melting and completed before pouring.

Once the molten metal reaches the targeted pouring temperature uniformly, pouring must be conducted immediately. Holding the molten metal at the pouring temperature for a long period of time can result in significant oxidation and loss of certain key alloying elements. The pouring spout of the crucible was preheated before pouring, using a propane blow torch to avoid rapid cooling of the molten metal during pouring.

## 8. Post-treatment

### *8.1 Post-casting cleaning*

After casting, the molds filled with metal were allowed to cool to room temperature in an ambient environment. Then the ceramic shell was removed. Figure 21 shows the obtained as-cast trees. Each casting tree produced multiple workpieces. The workpieces were then cut off from the "tree" for cleaning and inspection. Figure 22 shows the as-cast parts that were cut from the cast trees in Figure 21. As mentioned previously, to ensure the required tolerance, holes in the parts still required machining after casting. Therefore, machining the holes is also a viable approach and has been used in the designs shown in Figure 22 (a) and (b).

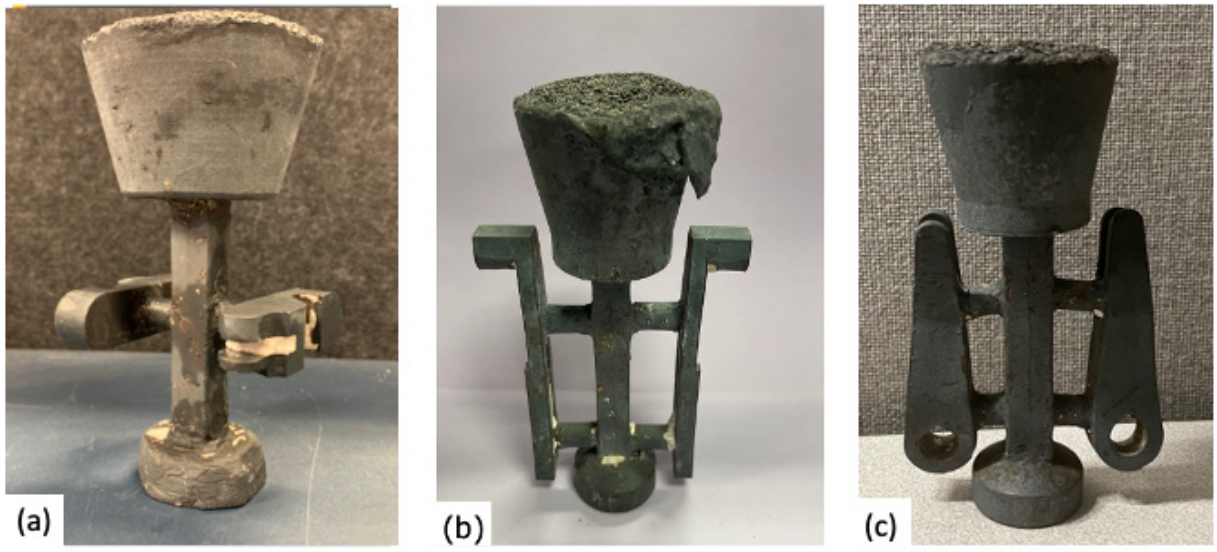


*Figure 21. As-cast casting trees (a) Part#12314649 casting tree assembly; (b) Part#12446263 casting tree assembly; (c)Part#154072 casting tree assembly.*

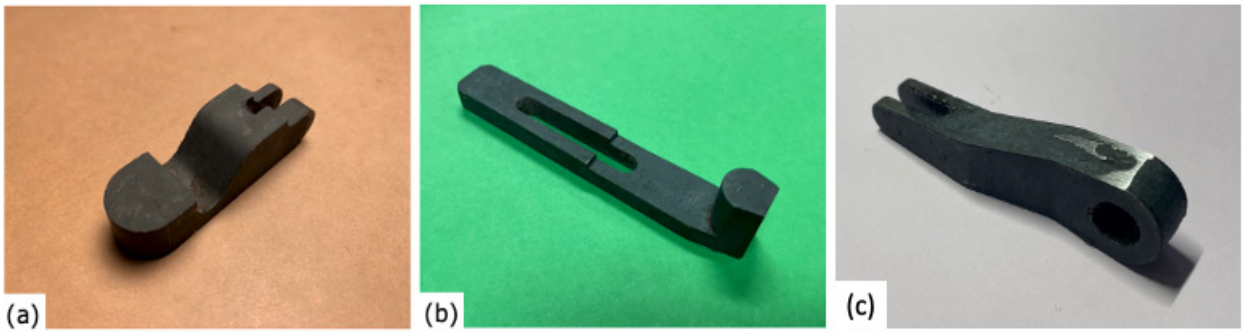


*Figure 22. As-cast parts cut from casting tree (a) Part#12314649; (b) Part#12446263; (c) Part#154072.*

*8.2 Hardness and heat treatment*

The hardness of the as-cast Part #12314649 product was measured to be 36.1 Rockwell hardness (HRC). To reach the specified target hardness of 30-35 HRC, and to eliminate residual stress in as-cast product, a standard heat treatment process was conducted [5]. The heat-treatment process included normalization at 860°C for 1 hour, followed by quenching in water and tempering at 650°C for 1 hour. After heat treatment, the hardness of the final product became 33 HRC.

The hardness of the as-cast Part #12446263 product was measured to be 39.2 HRC. To reach the specified target hardness of 32-38 HRC, as cast Part #12446263 was quenched from 860°C and tempered at 450°C for 1 hour. After heat treatment, the hardness of the final product was 36 HRC.

It is worth pointing out that the heat-treatment process should be designed uniquely for a specific alloy and specific hardness.

The design of Part #154072 does not specify the required hardness.

## 9. Characterization and inspection

*9.1 Chemical composition*

According to the part drawing and specification provided by the DEVCOM-GVSC, the required material for Part #12314649 is 4140 or 8640 alloy steel. The waste materials were selected by the established blending model from the waste metal database. During melting, based on the in-

situ composition monitoring results by portable OES, 0.43 pound of pure Mn flakes was added to adjust the Mn concentration. In addition, 0.32 pound of Ferrosilicon was added to increase the Si concentration, and 2.5 pounds of cast iron were also added to increase the C concentration. It is well known in steel making that Mn, Si, and C are elements that can be easily lost during melting. As shown in Table 7, the chemical composition of the final product complies well with the required composition range for AISI 4140 and AISI 8640.

*Table 7. Chemical composition of fabricated parts and target composition range.*

| | | C | Mn | Si | Cr | Mo | Ni | S | P | DI | CE |
|---|---|---|---|---|---|---|---|---|---|---|---|
| **Part #12314649 Target composition** | 4140 | 0.38-0.43 | 0.75-1.0 | 0.15-0.3 | 0.8-1.1 | 0.15-0.25 | / | 0-0.04 | 0-0.0035 | 4.44-8.38 | 0.64-0.87 |
| | 8640 | 0.38-0.43 | 0.75-1.0 | 0.15-0.35 | 0.4-0.6 | 0.15-0.25 | 0.4-0.7 | 0-0.04 | 0-0.0035 | | |
| **Product** | | 0.41 | 0.805 | 0.15 | 1.12 | 0.215 | 0.53 | 0.039 | 0.023 | 8.26 | 0.85 |
| **Part #12446263 Target composition** | 4130 | 0.28-0.33 | 0.4-0.6 | 0.15-0.3 | 0.8-1.1 | 0.15-0.25 | / | 0-0.04 | 0-0.0035 | | |
| | 4140 | 0.38-0.43 | 0.75-1.0 | 0.15-0.3 | 0.8-1.1 | 0.15-0.25 | / | 0-0.04 | 0-0.0035 | 2.51-6.38 | 0.54-0.91 |
| | 4142 | 0.4-0.45 | 0.75-1.1 | 0.15-0.3 | 0.8-1.1 | 0.15-0.25 | / | 0-0.04 | 0-0.0035 | | |
| **Product** | | 0.29 | 0.64 | 0.05 | 0.87 | 0.16 | 0.14 | 0.03 | 0.02 | 2.94 | 0.58 |
| **Part #154072 Target composition** | 1010-1025 | 0.08-0.28 | 0.3-0.6 | / | / | / | / | 0-0.05 | 0-0.04 | 0.086-0.45 | 0.13-0.38 |
| **Product** | | 0.176 | 0.575 | 0.488 | 0.127 | 0.012 | 0.108 | 0.03 | 0.023 | 0.28 | 0.27 |

Part #12446263 was designed to be made of 4130-4142 chromium-molybdenum alloy steel. As shown in Table 7, the chemical composition of the final product, except for silicon, fell within the specified range. Silicon is usually added in alloy steels during melting to act as a deoxidizer [6, 7]. The lack of silicon could result in fine air bubbles in the final product. In the casting process, pure aluminum was also added as a final deoxidizer. Additionally, carbon and manganese in the alloy function as deoxidizer [6]. As shown in the representative microstructure image in Figure 23, no air bubbles were observed in the final product.

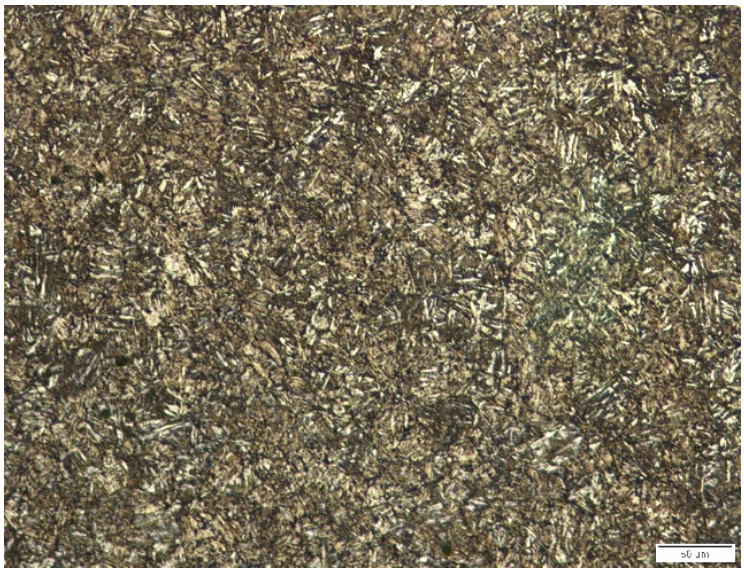

*Figure 23. Microstructure image of final product Part #12446263.*

Silicon in the steel alloy is expected to increase the hardenability and strength of the steel product [7]. Other alloying elements can serve a similar function, such as carbon, manganese, chromium, and molybdenum. Therefore, the Ideal Critical Diameter (DI) and Carbon Equivalent (CE) were developed and widely used to reliably gauge the properties and performance of steel alloy with multiple alloying elements. As shown in Table 7 the DI and CE values of the final product were calculated and both were within the expected ranges [8-10]. This result confirms that the effect of slightly lower than expected silicon content on hardenability has been compensated by other alloying elements. In addition, the mechanical properties of the final product can be adjusted by heat treatment to reach the target value. Therefore, the content of silicon in the final product was not considered to be a significant concern.

Part #154072 was designed to be made of 1010-1025 carbon steel. As shown in Table 7, the chemical composition of the final product fell within the specified range.

*9.2 Dimension inspection*

After heat treatment, the parts were sandblasted for final surface finishing. The final products are shown in Figure 24. The key dimensions of the printed patterns and cast parts were measured and summarized in the table insets in Figures 25, 26, and 27, correspondingly. The results show that all key dimensions of the final product were within required tolerance.


*Figure 24. Final parts (a) Part#12314649; (b) Part#12446263; (c) Part#154072.*

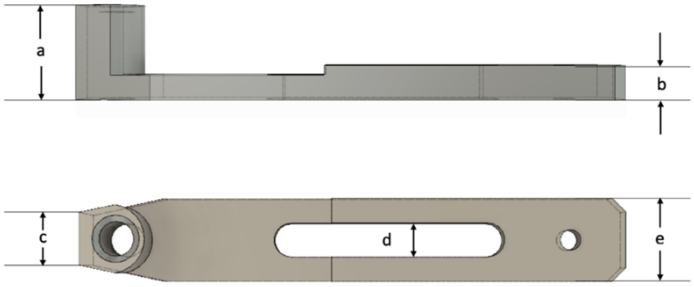


| Dimension (in.) | a | b | c | d | e |
|---|---|---|---|---|---|
| Design value ± tolerance | 0.69±0.03 | 0.25±0.03 | 0.38±0.03 | 0.252±0.03 | 0.62±0.03 |
| 3D printed pattern | 0.78 | 0.32 | 0.39 | 0.26 | 0.64 |
| Cast part | 0.698 | 0.269 | 0.382 | 0.257 | 0.625 |

*Figure 26. Part #12446263 final product dimension inspection and comparison.*

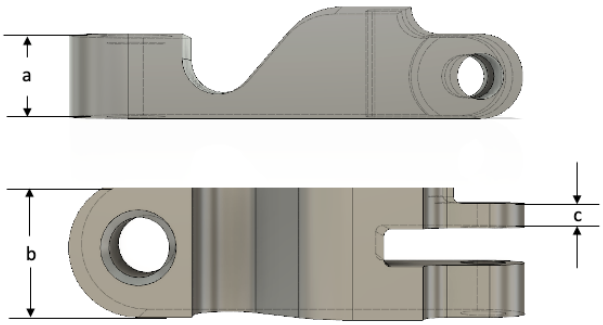


| Dimension (in.) | a | b | c |
|---|---|---|---|
| Designed value ± tolerance | 0.38 ± 0.01 | 0.63 ± 0.01 | 0.11 ± 0.01 |
| 3D printed pattern | 0.415 | 0.649 | 0.113 |
| Cast part | 0.371 | 0.630 | 0.112 |

*Figure 25. Part #12314649 final product dimension inspection of the final product.*

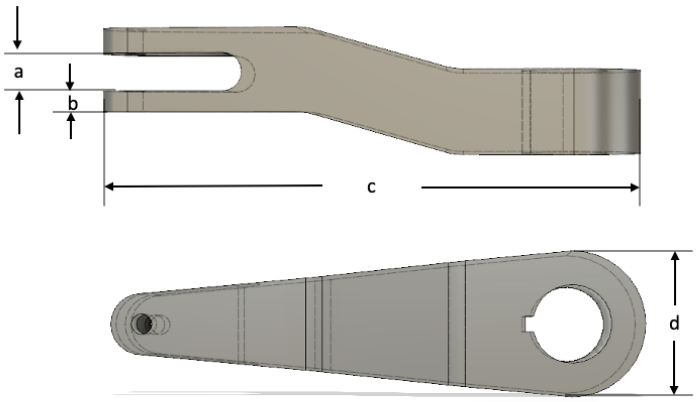


| Dimension (in.) | a | b | c | d |
|---|---|---|---|---|
| Designed value ± tolerance | 0.225 ± 0.015 | 0.125 ±0.015 | 3.25 ±0.015 | 0.875 ± 0.015 |
| 3D printed pattern | 0.232 | 0.129 | 3.347 | 0.903 |
| Cast part | 0.224 | 0.128 | 0.324 | 0.869 |

*Figure 27. Part #154072 final product dimension inspection of the final product.*

## 10. Summary

In summary, three demonstration pieces have been successfully produced from waste metals to verify the integration of formulation of alloys with the SLA enabled casting. The established manufacturing process is proven to be versatile.

## 11. Reference

[1] 3D Systems, Inc. ProJet™ 6000 3D Professional Printer, https://infocenter.3dsystems.com/product-library/sites/default/files/printers/projet-6000/ProJet%206000%20User%20Guide%20(Part%20No.%20283789-00,%20Rev.%20E).pdf

[2] Formlabs, Form 2 Tech Specs, https://formlabs.com/3d-printers/form-2/tech-specs/

[3] Sabau, Adrian S. "Alloy shrinkage factors for the investment casting process." *Metallurgical and Materials Transactions B* 37.1 (2006): 131-140.

[4] Sabau, Adrian S., and Srinath Viswanathan. "Material properties for predicting wax pattern dimensions in investment casting." *Materials Science and Engineering: A* 362.1-2 (2003): 125-134.

[5] Totten, George E., ed. *Steel heat treatment: metallurgy and technologies*. CRC press, 2006.

[6] Xiao, Wei, Min Wang, and Yanping Bao. "The research of low-oxygen control and oxygen behavior during RH process in silicon-deoxidization bearing steel." *Metals* 9, no. 8 (2019): 812.

[7] Song, E. J., D. W. Suh, and H. K. D. H. Bhadeshia. "Oxidation of silicon containing steel." *Ironmaking & Steelmaking* 39.8 (2012): 599-604.

[8] ASTM. ASTM A255 Determining the Hardenability of Steel. ASTM International.

[9] Kasuya, T., and N. Yurioka. "Carbon equivalent and multiplying factor for hardenability of steel." *WELDING JOURNAL-NEW YORK-* 72 (1993): 263-s.

[10] Najafi, H., J. Rassizadehghani, and S. Norouzi. "Mechanical properties of as-cast microalloyed steels produced via investment casting." *Materials & Design* 32.2 (2011): 656-663.